Deformation Behavior of Aluminum Bicrystals

By *Jui-Chao Kuo*, *Stefan Zaefferer*, *Zisu Zhao*, *Myrjam Winning*, and *Dierk Raabe**

Introduction: Grain boundaries are natural obstacles to the motion of dislocations during plastic straining of crystalline matter. As such, they may be the cause of grain-scale heterogeneity in terms of the mismatch of the elastic–plastic strain rate, internal stress, and crystallographic reorientation rate fields. Investigating such non-homogeneity systematically as a function of the grain boundary character under well-defined mechanical boundary conditions is important for a better understanding of grain-scale and grain-boundary micromechanics as well as the development of the micro- and nanoscale texture.

A hierarchical approach to studying grain-scale plastic heterogeneity consists in investigating the influence of isolated grain boundaries (bicrystals),[1–5] triple junctions (tri-crystals),[6,7] and simple grain boundary networks (oligocrystals)[8–11] under well-defined external loading conditions.

Early investigation of bicrystal deformation by Livingston and Chalmers[1] showed that at least four slip systems are required to explain the macroscopic plastic incompatibility observed at the boundary. The additional operation of second slip systems, due to elastic incompatibility at the grain boundary, was suggested by Hook and Hirth.[3,4] Both these studies focused on intergranular incompatibilities, i.e., on plastic and elastic incompatibility across the grain boundary. Rey and Zaoui[2,5,8] have shown that the internal stress due to intragranular incompatibilities at the grain boundary results in additional slip systems as well as pronounced hardening.

Most previous studies addressed essentially the question of elastic–plastic incompatibility at grain boundaries on a mesoscopic scale. A somewhat different approach has been adopted in this work as the spatial distribution of the plastic strain and the texture evolution at grain boundaries have been investigated on different scales, ranging from nanoscale texture determination to micro- and macroscopic measurements of the overall strain distribution within the surface of the sample. This scale-bridging experimental approach offers a better survey of the influence of the heterogeneous conditions imposed by the respective contact and loading situations and their influence on the local microstructure.

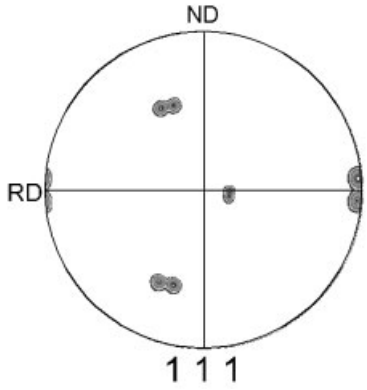

Fig. 1. {111} pole figure of the undeformed bicrystal with a symmetrical ⟨112⟩ tilt grain boundary and an initial misorientation of 8.7°.

Figure 1 shows the {111} pole figure of the initial specimen, an aluminum bicrystal with a symmetrical ⟨112⟩ tilt boundary with an initial misorientation of 8.7°, prior to mechanical loading. Plane strain compression experiments were carried out in a channel die setup and the specimen surface analyzed by photogrammetry between subsequent straining steps.

Experimental: Sample Preparation and Deformation Setup: An aluminum bicrystal with a symmetrical ⟨112⟩ tilt boundary and an initial misorientation of 8.7° was grown by a modified Bridgman technique. Plane strain compression experiments were carried out at a strain rate of 1.7×10^{-5} s^{-1} in a channel die setup, as shown schematically in Figure 2b. The sample is loaded along the compression direction (ND) and it expands in the elongation direction (RD). The front sides of the channel prevent displacements along the transverse direction (TD). During deformation, the normal of the grain boundary was parallel to the compression direction (ND), as shown in Figure 2a. The sample had a cross section of 17 mm × 20 mm and was 4 mm thick. In order to reduce frictional effects and protect the gray-scale pattern on the specimen surface as required for the photogrammetry analysis between the subsequent straining steps, the specimen was wrapped in a 80 μm thick poly(tetrafluoroethylene) (Teflon) foil.

Sample Characterization: Prior to deformation, the ND-RD (ND: compression direction, RD: elongation direction) sample surface was mechanically polished and the initial orientations were determined using automatic crystal orientation mapping (ACOM) by automatic analysis of electron backscattering diffraction (EBSD) patterns by scanning electron microscopy (SEM). Subsequently, a fine white color spray was applied on the polished surface in order to eliminate gleaming. Tiny dots of black color were then sprayed on the white background. This pattern gave excellent contrast for pattern recognition. Plane strain compression was performed in steps of about 5 % engineering plastic reduction up to a total thick-

[*] *Prof. D. Raabe, J.-C. Kuo, Dr. S. Zaefferer, Dr. Z. Zhao*
Max-Planck-Institut für Eisenforschung
Max-Planck-Strasse 1, D-40237 Düsseldorf (Germany)
E-mail: raabe@mpie.de
Dr. M. Winning
Institut für Metallkunde und Metallphysik, RWTH Aachen
Kopernikusstrasse 14, D-52056 Aachen (Germany)
Dr. Z. Zhao
Massachusetts Institute of Technology
77 Massachusetts Avenue Cambridge, MA 02139-4307 (USA)

 DOI: 10.1002/adem.200300372

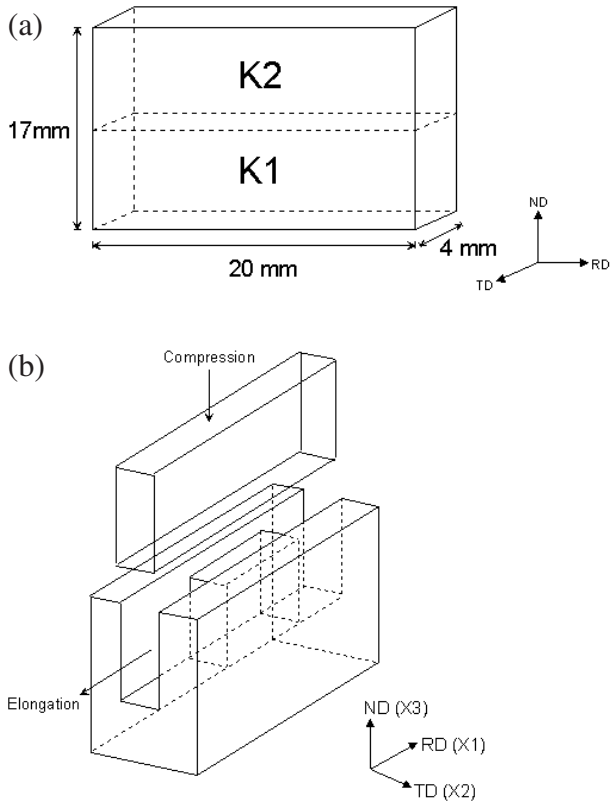

Fig. 2. Schematical drawing of the bicrystal a) and of the experimental set-up b).

ness reduction of 30 %. After each deformation step, including the initial undeformed state, the color patterns on the sample surface were recorded as digital images by use of a high resolution charge-coupled device (CCD) camera. After 30 % deformation, the deformed sample surface was once again mechanically polished and a final orientation mapping was measured by ACOM mapping the entire surface using a lateral step size of 100 μm. In addition, high-resolution orientation maps were measured close to the grain boundary and in the interior of the abutting crystals using a step size of 70 nm on 300 μm × 100 μm areas.

The plastic strain was determined by photogrammetry. The central feature of this technique is a procedure to quantify the match between an image (pattern) of the undeformed state and that of the deformed state in terms of a correlation coefficient *C*. The distribution of the gray-scale values of a rectangular area in the pattern taken from the undeformed state corresponds to that of the same area in the deformed state if *C* assumes a minimum. The correlation coefficient *C* is defined as

$$C = 1 - \int_{\Delta S} f_s(x_s, y_s) f_d(x_d, y_d)\, dxdy \Big/ \sqrt{\int_{\Delta S} f_s(x_s, y_s)^2\, dxdy \int_{\Delta S} f_d(x_d, y_d)^2\, dxdy} \quad (1)$$

where ΔS is the inspected area of the correlation pattern in the initial image, and $f_s(x_s,y_s)$ and $f_d(x_d,y_d)$ are the gray-level values in the reference and deformed regions, respectively [9,10,12]. After the matching procedure, the displacement field on the surface can first be derived and, from this, the in-plane strain distribution can also be deduced from the corresponding coordinates in the initial and deformed states. The in-plane plastic strain mapping can be categorized into two different types, an accumulated and an incremental strain mapping. The former is obtained by comparing the image after each deformation step with respect to the initial image. The latter is determined by comparing the images taken before and after each deformation step.

The plastic von Mises strain distribution was calculated from the strain components. After 5 % thickness reduction, the distribution of the plastic von Mises strain was quite homogeneous (Fig. 2a). After 30 % engineering thickness reduction, both crystals revealed macroscopic deformation bands that do not correspond to crystallographic slip directions (Fig. 2b). Although the initial orientations of both crystals were symmetrical with respect to the grain boundary plane and the compression direction, the strain distributions in the two crystals were quite different. While the upper crystal showed high accumulated stresses, the lower one was

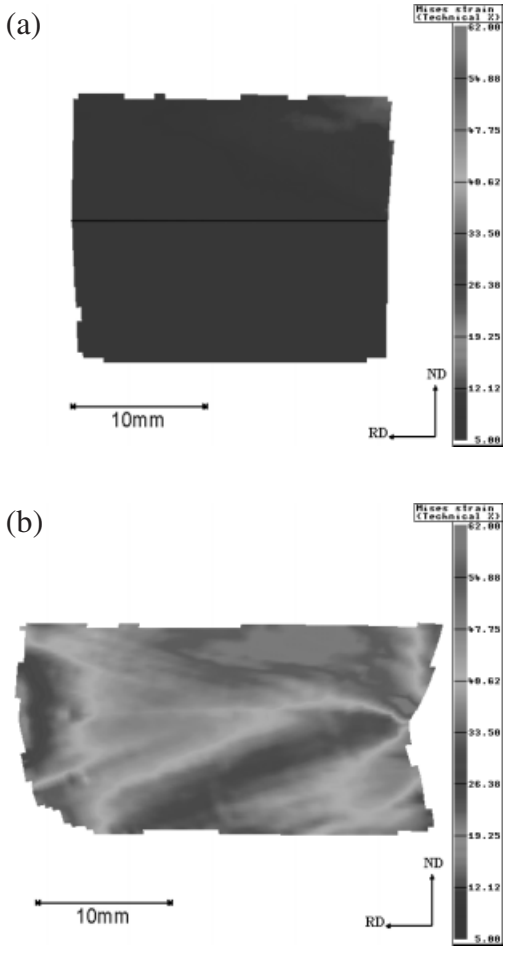

Fig. 3. Spatial distributions of the von Mises strain obtained by measurement a) after 5 % and b) after 30 % deformation.

ADVANCED ENGINEERING MATERIALS

much less deformed. The above results suggest that the channel die experiment promotes heterogeneous deformation patterns, which are to a large extent influenced by the form of the sample and the amount of friction between tool and sample.

Crystal orientation maps were measured close to the grain boundary and inside the two abutting crystals in areas that had undergone similar accumulated plastic straining (Figure 3). The results are shown in Figure 4 in the form of misorientation maps, where the color coding corresponds to the angular deviation of a given point with respect to each initial orientation. All three areas show similar microstructures consisting of two sets of parallel bands of similar orientations. The arrangement of the parallel nanoscaled bands in each of the three mappings establishes a highly lamellar microstructure in which the in-grain orientation systematically fluctuates in the form of forward and backward orientation changes. The resulting overall orientation spread arising from such microtexture patterning can be observed in the form of orientation traces in the {111} pole figures given in Figure 5. A comparison of the texture maps taken from the grain interiors (Figs. 4a and 4c) with that taken across the grain boundary (Fig. 4b) shows that the separation of these bands is smaller in the vicinity of the grain boundary. Moreover, as compared to the misorientations in the grain interiors, the misorientations in the immediate vicinity of the grain boundary are smaller.

Figures 5a and b show the distinct {111} pole figures of areas near the grain boundary and in the interiors of the two

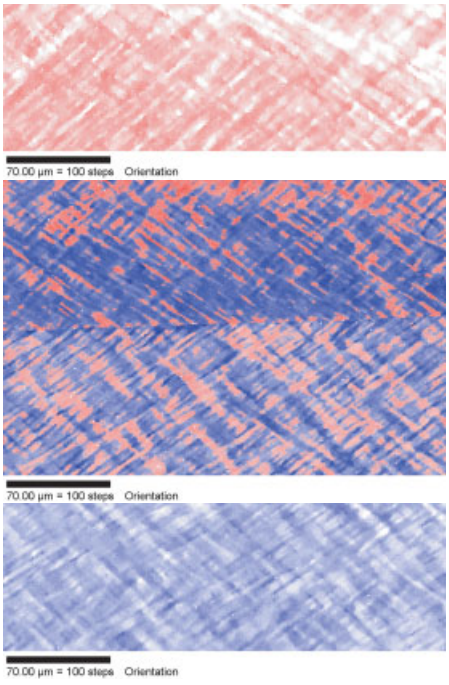

(a) crystal K2, 2 mm away from the grain boundary

(b) crystal K2 and K1 at grain boundary, 12 mm from the left top, as shown in Figure 3b

(c) crystal K1, 2 mm away from the grain boundary

Fig. 4. Microtexture mappings in regions close to the grain boundary with similar strain conditions in the 30 % deformed bicrystal (EBSD step size: 700 nm, color coding represents misorientation mapping selected separately in each area according to the local range in orientation change with respect to each initial orientation of crystal K1 and crystal K2).

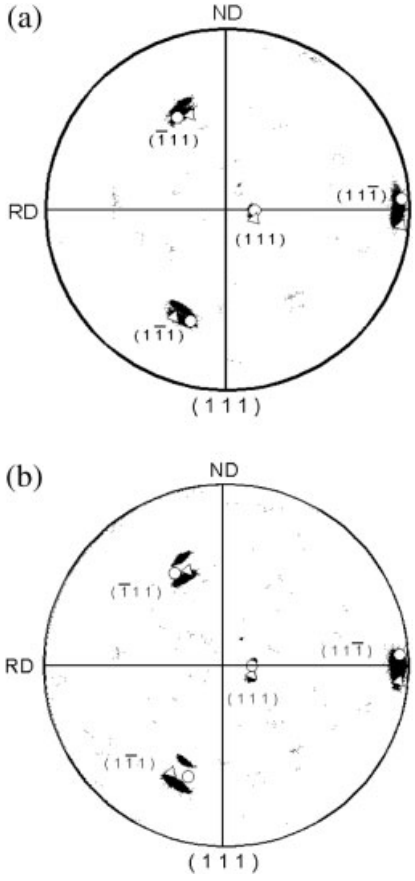

Fig. 5. {111} pole figures measured by EBSD in the immediate vicinity of the grain boundary a) and in the interiors of both crystals b) in the 30 % deformed bicrystal (○: initial orientation of crystal K1, △: initial orientation of crystal K2). The data clearly show that the grain interiors reveal a mutual misorientation after straining larger than that in areas close to the interface.

crystals obtained from the electron backscattering diffraction (EBSD) data measured. The data clearly show that, after straining, the grain interiors reveal a mutual misorientation larger than that of the areas close to the interface. Compared to the initial orientations before deformation, the areas close to the grain boundary have rotated towards each other, while the areas at a distance of 2 mm to the grain boundary have increased their misorientation. This is consistent with the observations of the misorientation gradients mentioned above.

In conclusion, we have investigated the deformation behavior of an aluminum bicrystal with a symmetrical ⟨112⟩ tilt boundary and an initial misorientation of 8.7°. The specimen was compressed in a channel die to 30 % engineering thickness reduction at room temperature. The lateral fields of the crystallographic lattice rotations and plastic strains were jointly characterized and the plastic strain distribution was determined by photogrammetry. We observed a high degree of heterogeneity in the strain in the symmetric bicrystal, i.e., an asymmetric strain distribution was found although the crystal orientations and the boundary plane were symmetric with respect to loading. Crystal lattice rotations were determined by means of EBSD in a high-resolution scanning electron microscope. It was found that the crystals rotated to-

wards each other close to the grain boundary. In contrast, the grain interiors revealed an increase in misorientation.

Received: May 13, 2003

[1] J. D. Livingston, B. Chalmers, *Acta Metall.* **1957**, *5*, 322.
[2] C. Rey, A. Zaoui, *Acta Metall.* **1980**, *28*, 687.
[3] R. E. Hook, J. P. Hirth, *Acta Metall.* **1967**, *15*, 535.
[4] R. E. Hook, J. P. Hirth, *Acta Metall.* **1967**, *15*, 1099.
[5] C. Rey, A. Zaoui, *Acta Metall.* **1982**, *30*, 523.
[6] V. Randle, N. Hansen, D. Juul Jensen, *Philos. Mag. A* **1996**, *73*, 265.
[7] R. K. Davies, V. Randle, *Mater. Sci. Eng. A* **2000**, *283*, 251.
[8] C. Rey, *Rev. Phys. Appl.* **1988**, *23*, 491.
[9] D. Raabe, M. Sachtleber, Z. Zhao, F. Roters, S. Zaefferer, *Acta Mater.* **2001**, *49*, 3433.
[10] M. Sachtleber, Z. Zhao, D. Raabe, *Mater. Sci. Eng. A* **2002**, *336*, 81.
[11] F. Delaire, J. L. Raphanel, C. Rey, *Acta Mater.* **2000**, *48*, 1075.
[12] P. Vacher, S. Dumoulin, F. Morestin, S. Mguil-Touchal, *Proc. Inst. Mech. Eng., Part C: J. Mech. Eng. Sci.* **1999**, *213*, 811.

High-Resolution EBSD Investigation of Deformed and Partially Recrystallized IF Steel

By *Ingo Thomas*,* *Stefan Zaefferer*, *Frank Friedel*, and *Dierk Raabe*

Abstract: The recrystallization of titanium-alloyed interstitial-free steel (IF steel) has been investigated by high-resolution electron backscattered diffraction (EBSD) measurements and transmission electron microscopy (TEM) observations. The deformed microstructure of the cold rolled material can be subdivided into three different groups. These three types of microstructure are characterized by their orientations and internal local misorientations. The development of these three regions during recrystallization annealing has been observed. Nucleation from γ-fiber orientations but also from other orientations was found. Comparison of EBSD and TEM results indicates some limitations of high-resolution EBSD measurements concerning the observation of subgrain structures.

[*] *I. Thomas, Dr. S. Zaefferer, Prof. D. Raabe*
Max-Planck-Institut für Eisenforschung
Max-Planck-Strasse 1, D-40237 Düsseldorf (Germany)
E-mail: thomas@mpie.de
I. Thomas, Dr. F. Friedel
Thyssen Krupp Stahl
D-47161 Duisburg (Germany)

Motivation: IF steels are mainly used as sheets for deep-drawing applications (car bodies, cans etc.) for which a high *r* value (ratio of strain in width direction to that in thickness direction) is required, in order to reduce thinning. It is well known that a high *r* value is related to a high fraction of crystals with a <111>//ND crystal orientation fiber (called γ-fibre).[1] Homogeneous occupation of this orientation fiber also leads to a low anisotropy within the sheet plane. As the γ-fibre is mainly created during recrystallization after heavy cold rolling, this process is of high significance for applications of IF steel. Another important crystal orientation fiber is <110>//RD. The latter is called α-fibre and is formed typically when rolling bcc metals.

The problem with recrystallization of IF steels is related to the heterogeneity of the process. Figure 1 shows an example of a recrystallization process taken from a work by Raabe.[2] In this case, recrystallization evolved in a strongly heterogeneous way throughout the material. In the lower part of the picture, recrystallization has not taken place at all, whereas, in the upper part, two different recrystallization regimes are visible, showing different grain sizes. All three different kinds of microstructure, as expected, display different mechanical behaviors and lead to unwanted surface effects (such as orange peel structure) during deep-drawing operations. In order to understand and predict phenomena such as the one shown in Figure 1, it is necessary to improve our knowledge of the recrystallization process. The basic problem in this context is understanding which features of the microstructure enable nucleation for the recrystallization process.

It has been well established that the ability to form a nucleus is strongly dependent on the orientation of the material[3] and it is therefore important to study the local orientation distribution and microstructure with high spatial resolution. EBSD applied in a high-resolution scanning electron microscope (SEM) is the most appropriate tool for this task as it gives both high resolution and large observable areas. In this communication we describe a study of the recrystallization progress in IF steel. The deformed and several partially recrystallized states are characterized mainly by EBSD investigations. TEM is also used to study details of the deformed microstructure.

Experimental: The EBSD measurements were carried out with a field emission SEM (JEOL JSM 6500 F) equipped with a TSL EBSD system and a Digiview CCD camera. The SEM was operated at an accelerating voltage of 15 kV. Samples were prepared by grinding and polishing. The samples were etched for a few seconds, using a solution of 10:1 H_2O_2:HF. The etching process was stopped by using pure H_2O_2. As the microstructure of deformed IF steel shows quite small structures, the EBSD measurements were performed with a step size of 0.1 or 0.15 μm. In order to the use of wrongly indexed orientations, data points with a confidence index lower than

  DOI: 10.1002/adem.200300373